Asian Journal of Chemistry; Vol. 38, No. 6 (2026), 1515-1523
ASIAN JOURNAL OF CHEMISTRY
https://doi.org/10.14233/ajchem.2026.35831

Hetero Atom doped Carbon Quantum Dots as Smart Materials for Corrosion Application

G. RUBY and P. BHAVANI*

PG and Research Department of Chemistry, R.V. Government Arts College, Chengalpattu-603001, India

*Corresponding author: E-mail: bhavaniperumal4@gmail.com

Received: 27 February 2026 *Accepted*: 30 April 2026 *Published online*: 31 May 2026 AJC-22377

In this work, nitrogen and boron co-doped carbon quantum dots (N,B-CQDs) were synthesized by a hydrothermal method and evaluated as fluorescence-based probes for corrosion monitoring. The incorporation of nitrogen and boron modified the electronic structure and surface chemistry of the CQDs, resulting in enhanced photoluminescence stability, strong fluorescence intensity and improved environmental stability. The synthesized N,B-CQDs exhibited uniform spherical morphology (4-8 nm) with bright blue fluorescence under UV irradiation. The structural, optical and surface properties of the N,B-CQDs were characterized using TEM, XRD, UV-visible spectroscopy, photoluminescence spectroscopy, FTIR, XPS and TCSPC analyses. The N,B-CQDs showed high sensitivity and selectivity toward Fe^{3+} ions and pH variation, both of which are important indicators of corrosion processes. Fluorescence quenching occurred predominantly through static interaction with partial inner filter effect contribution. In addition, the CQDs exhibited reversible pH-responsive fluorescence behaviour suitable for repetitive monitoring. The results demonstrate that N,B-CQDs are promising fluorescent nanoprobes for sensitive, non-destructive and real-time corrosion monitoring applications.

Keywords: Carbon quantum dots, Corrosion monitoring, Electronic structure, Surface chemistry, Photoluminescence.

INTRODUCTION

Corrosion is a major challenge affecting the durability, safety and operational efficiency of metallic materials used in construction, transportation, energy systems, marine infrastructure and industrial processing units. The gradual deterioration of metals through electrochemical reactions results in significant economic losses and structural failures worldwide [1,2]. Early-stage corrosion is often difficult to detect because the process initiates at localized interfaces before visible surface damage occurs. Conventional corrosion monitoring techniques including electrochemical impedance spectroscopy, weight-loss analysis, surface microscopy and ultrasonic testing, generally require sophisticated instrumentation, direct surface contact and complex sample preparation [1]. In addition, many of these methods are unsuitable for continuous, *in situ* and real-time monitoring under harsh environmental conditions [3,4]. Therefore, the development of sensitive, rapid and non-destructive sensing platforms for corrosion detection has become increasingly important.

Fluorescence-based sensing has emerged as an effective analytical strategy owing to its high sensitivity, rapid response, excellent signal resolution and visual detectability [5]. In recent years, carbon quantum dots (CQDs) have attracted substantial interest as fluorescent nanomaterials because of their unique optical and physico-chemical properties including tunable photoluminescence, high aqueous dispersibility, low toxicity, chemical inertness and environmental compatibility [5-7]. CQDs also possess abundant surface functional groups that facilitate interaction with metal ions and environmentally responsive species, making them attractive candidates for sensing and monitoring applications. Recent studies have demonstrated the applicability of CQDs in ion sensing, bioimaging, environmental analysis and anti-counterfeiting technologies due to their stable fluorescence characteristics and facile synthesis routes [7-9].

Despite these advantages, undoped CQDs frequently exhibit limitations such as low fluorescence quantum yield, excitation-dependent emission instability and susceptibility to environmental quenching, which restrict their practical use in corrosion-monitoring systems [8,9]. Surface defects and uncontrolled electron-hole recombination further reduce their sensing efficiency under variable pH and ionic conditions. To overcome these limitations, heteroatom doping has emerged as an effective strategy to tailor the electronic structure and surface chemistry of CQDs. Nitrogen doping introduces electron

rich sites and improves radiative recombination efficiency, whereas boron doping generates electron-deficient centers that enhance charge separation and suppress non-radiative decay pathways [10,11]. Simultaneous co-doping with nitrogen and boron develops a balanced donor-acceptor electronic system that significantly improves fluorescence intensity, quantum yield, surface reactivity and environmental stability.

Corrosion processes are generally accompanied by localized pH fluctuations, release of iron ions and interfacial electron-transfer reactions [12]. These physico-chemical changes provide suitable targets for fluorescence-based sensing using heteroatom-doped CQDs. Recent investigations have shown that boron-containing functional groups exhibit strong coordination interactions with Fe^{3+} ions, while nitrogen functionalities promote efficient electron transfer and fluorescence modulation [13-15]. Such synergistic interactions enhance the sensitivity and selectivity of N,B doped CQDs toward corrosion-associated species. In addition, pH-responsive fluorescence behaviour of co-doped CQDs enables real-time monitoring of localized acidification during corrosion propagation.

Based on these considerations, the present work focuses on the hydrothermal synthesis of nitrogen and boron doped carbon quantum dots (N,B-CQDs) and their application as fluorescence probes for corrosion monitoring. The synthesised N,B-CQDs were systematically characterized using TEM, XRD, FTIR, XPS, UV-visible spectroscopy, photoluminescence analysis and fluorescence lifetime measurements. Their sensing performance toward Fe^{3+} ions and pH variation were investigated to evaluate their suitability for sensitive, reversible and real-time corrosion detection systems.

EXPERIMENTAL

Without additional purification, citric acid (carbon source), urea (nitrogen source) and boric acid (boron source) were used. Lemon peel extract was employed as a green reducing and capping agent. Iron(III) chloride and copper(II) sulphate were used as model corrosion related metal ions. Triple distilled water was used to prepare each solution.

Preparation of N,B doped CQDs: N,B-CQDs were prepared by hydrothermal method [13,14]. A homogenous solution was prepared by dissolving citric acid, urea and boric acid in distilled water with lemon peel extract. The reaction mixture was transferred to a Teflon-lined autoclave and heated at 200 ºC for 6 h. After cooling, the subjected product was filtered and centrifuged to remove larger particles, The prepared N,B co-doped carbon quantum dots solution was stored at 4 ºC for subsequent use.

Measurement of quantum yield of N,B doped CQDs: The fluorescence quantum yield (QY, Φ) is defined as the ratio of the number of photons emitted to the number of photons absorbed. In the present study, the quantum yield of hydrothermally synthesised N,B co-doped carbon quantum dots (N,B-CQDs) was determined using quinine sulphate as the reference standard (Φ_R = 0.55 in 0.1 M H_2SO_4) [15].

$$\Phi = \Phi_R \frac{I}{I_R} \times \frac{A_R}{A} \times \frac{\eta^2}{\eta_2^R}$$

where Φ is the quantum yield of the sample, Φ_R is the quantum yield of the reference standard, I and I_R are the integrated fluorescence emission intensities of the sample and reference, respectively, A and A_R represent the absorbance (optical density) of the sample and reference at the excitation wavelength, and η and η_R are the refractive indices of the solvents used for the sample and reference, respectively.

The quantum yield of N,B-CQDs was found to be 32% which is greater than that of conventional CQDs. Thus, the results confirm that nitrogen and boron co-doping produces a synergistic effect that enhances surface passivation, suppresses non-radiative recombination pathways and promotes efficient radiative emission [16-18].

Determination of Fe^{3+}: The fluorescence behaviour in N,B-CQDs) towards corrosion related metal ions was systematically investigated in order to assess the feasibility of N,B-CQDs for corrosion monitoring. Foreign ions *viz*. Mg^{2+}, Pb^{2+}, Ca^{2+}, Cu^{2+}, Mn^{2+}, Ni^{2+}, Hg^{2+}, Ba^{2+}, Cd^{2+}, Co^{2+}, Al^{3+}, Na^{+}, Ag^{+} and Fe^{3+} were all added separately to the N,B-CQDs solution (0.1 mg/mL) at a fixed concentration of 100 μM. Selectivity was evaluated by the fluorescence spectra and were recorded following a 5 min equilibration time. N,B-CQDs have a high selectivity for Fe^{3+} ions caused by corrosion processes as confirmed by the considerable fluorescence quenching that was induced by the Fe^{3+}, which is a key indicator for corrosion amongst all the tested ions.

Iron(III) solutions with concentrations ranging from 0 to 100 μM were added to the N,B-CQDs dispersion and the corresponding fluorescence intensity changes were measured in order to establish the quantitative corrosion monitoring capability. The observed linear relationship between fluorescence quenching efficiency and Fe^{3+} concentration indicates that N,B-CQDs serve as a sensitive tool for monitoring iron release during corrosion processes. The feasibility of the developed sensor was identified by its ability to detect Fe^{3+} in real aqueous environments for corrosion studies such as tap water, lake water which can simulate Industrial cooling water and natural exposure conditions. Fluorescence measurements were done using the N,B-CQDs probe after adding known amounts of Fe^{3+} (0, 10, 20, 30 and 50 μM) to the samples. All the experiments were performed at triplicate and the mean values with standard deviations confirmed good accuracy and reproducibility.

The sensor was then utilised for the analysis of Fe^{3+} containing solid samples in order to analyze the corrosion products from metallic materials. Iron supplement tablets, which contained 60 mg per tablet, were used as a model system. The samples were digested with conc. HNO_3 (1000 μL) and incubated for 2 h to release Fe^{3+} ions. The pH was then adjusted using 0.1 M NaOH. The fluorescence sensor based N,B-CQDs was used to measure the concentration of Fe^{3+}. The recovery experiments were conducted by the spiking additional Fe^{3+} (10 and 25 μM) and the calculated recovery rates and relative standard deviations (RSD) confirmed the reliability of the sensing platform for corrosion related iron detection. These results show that N,B-CQDs can serve as an efficient fluorescence based probe for real time corrosion monitoring by sensitively detecting Fe^{3+} ions released from iron containing materials in aqueous environments.

RESULTS AND DISCUSSION

Structural and morphological studies: The XRD diffraction pattern exhibited a broad diffraction peak around 24º, indicating the amorphous nature of the carbon framework with short-range graphitic ordering and confirming successful heteroatom incorporation. The broad diffraction feature suggests the presence of disordered carbon structures with low crystallinity, which is characteristic of carbon quantum dots [19-21]. The incorporation of nitrogen and boron atoms into the carbon matrix introduced defect sites and modified the electronic structure, thereby enhancing the optical properties and sensing performance of the N,B-CQDs. (Fig. 1a).

The TEM image (Fig. 1b-c) shows that the N,B-CQDs possess uniform spherical morphology with an average particle size 4 to 8 nm. The narrow size distribution contributes to consistent emission behaviour. Such a narrow and size distribution is highly advantage, as it reduces size dependent energy distribution and leads to stable and consistent emission behaviour. The absence of visible aggregation further confirmed their good dispersibility of the synthesised N,B-CQDs.

Surface functionalization and doping confirmation: The surface functional groups and chemical composition of the synthesised N,B-CQDs were analysed by FITR spectroscopy. The FITR spectrum exhibits several characteristics absorption bands such as broad beak at 3415 cm^{-1} corresponding to O-H and N-H stretching vibrations [22]. The other peaks at 1600, 1450, 1150, 1090 and 1045 cm^{-1} were assigned to the bending vibration of C=O, C-N, B-O-H, C-B, B-O-N, respectively and stretching vibration of C-B indicated that B and N atoms were successfully doped in B,N CQDs (Fig. 2a).

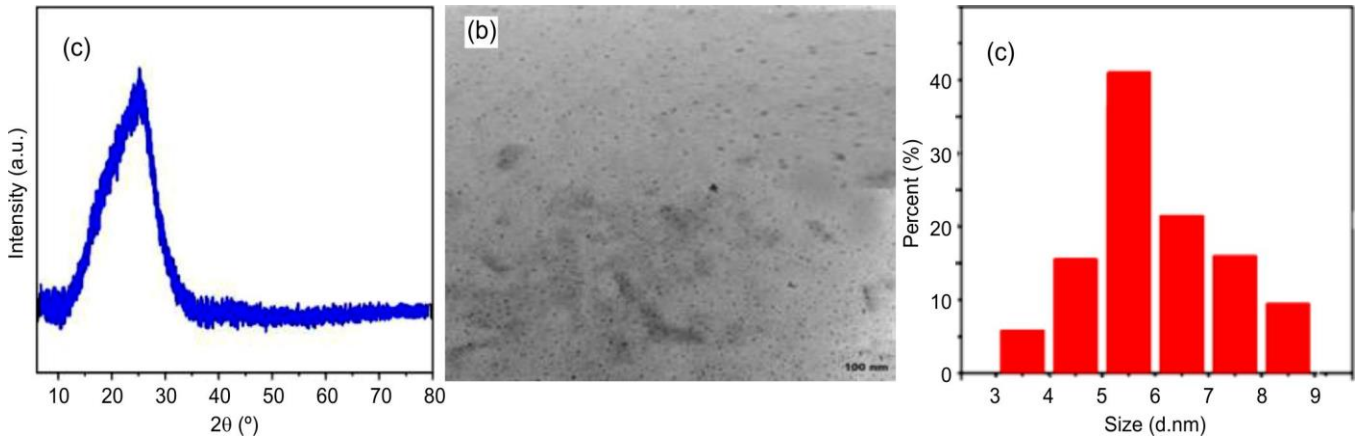

Fig. 1. (a) XRD spectrum, (b) TEM image and (c) size distribution chart of N,B-CQDs

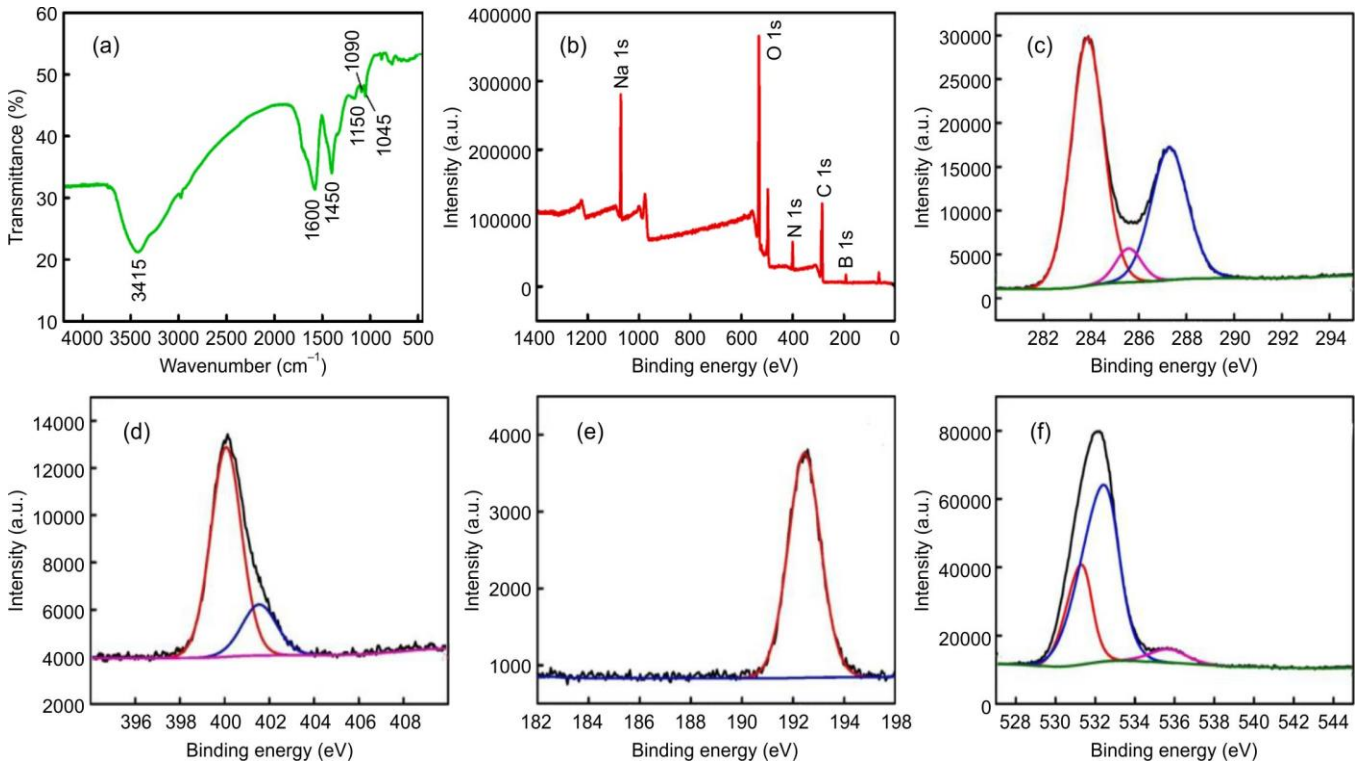

Fig. 2. (a) FITR spectrum, (b) XPS spectrum, (c) C_{1s}, (d) N_{1s}, (e) B_{1s} and (f) O_{1s} of N,B-CQDs

X-ray photoelectron spectroscopy (XPS) was used to investigate the elemental composition and chemical bonding states of the synthesised N,B-CQDs. It confirmed the presence of carbon, nitrogen, oxygen and boron as primary constituent elements of B,N CQDs from Fig. 2b. High resolution C 1s spectra show three peaks at 285.2 eV, 287.15 eV and 287.95 eV, which indicate C=C/C-C, C-O/C-N and C=O/C=N bonding environments respectively (Fig. 2c). The N 1s spectrum displays two distinct peaks at 400.4 eV and 400.95 eV corresponding to N-H and C-N/N-N bonding represents the successful nitrogen incorporation (Fig. 2d). The B 1s spectrum exhibits a characteristic peak at 191.95 eV is assigned to B-O bonding which confirmed the presence of boron containing functional groups (Fig. 2e). Furthermore, in the O1s spectrum, the peaks observed at 530.95 eV, 531.8 eV and 536.4 eV are attributed to C=O, C-O-C/C-OH and –OH bonding, respectively (Fig. 2f). FTIR and XPS analyses revealed that the surface of the N,B-CQDs was richly functionalised with oxygen-, nitrogen- and boron-containing groups, providing abundant active sites for interaction with metal and non-metal ions [23-25]. These surface functionalities significantly enhanced the sensing efficiency and corrosion monitoring capability of the N,B-CQDs.

Optical properties of B,N-CQDs: The UV-visible absorption spectrum of N,B-CQDs exhibited two prominent absorption bands at 245 and 320 nm (Fig. 3), corresponding to the π-π* transition of C=C and the n-π* transition of C=O functional groups, respectively. The N,B-CQDs displayed maximum fluorescence emission at 440 nm under an excitation wavelength of 350 nm and showed bright blue luminescence under UV irradiation at 360 nm, consistent with the observed colour coordinates [26,27]. The emission peak position remained nearly unchanged when the excitation wavelength (λ_{ex}) varied from 325 to 385 nm, while the fluorescence intensity reached its maximum around 360 nm excitation.

The excitation-dependent photoluminescence behaviour of the N,B-CQDs was further investigated by varying the excitation wavelength. An emission maximum around 420 nm (λ_{em}) was observed at an excitation wavelength of 330 nm (λ_{ex}) indicating the presence of multiple emissive trap states and surface heterogeneity (Fig. 3a-b). This behaviour is attributed to the different surface energy levels and radiative recombination pathways generated by N- and B-doping within the carbon quantum dot framework.

Comparison with undoped and doped CQDs: A controlled comparative study was carried out using undoped, N-doped, B-doped and N,B co-doped CQDs synthesised under identical conditions. The N,B-CQDs exhibited a significantly higher quantum yield and longer fluorescence stability than undoped and singly doped carbon quantum dots (Table-1). The enhanced emission intensity further confirmed the improved radiative recombination.

Fluorescence based corrosion monitoring: The fluorescence based corrosion monitoring mechanism used N,B-CQDs depends on the release of Fe^{3+} ions during the electrochemical corrosion of iron or steel surfaces in aqueous environment. Anodic dissolution of metallic iron in presence of oxygen and moisture produces Fe^{2+} ions, which are subsequently oxidised to Fe^{3+} ions under aerobic conditions. These Fe^{3+} ions move into the surrounding solution and act as a direct indicator of corrosion progression [31,32]. When Fe^{3+} ions are introduced into the N,B-CQDs sensing system, strong coordination interactions occur between Fe^{3+} ions and the surface functional groups of the quantum dots such as hydroxyl (-OH), carboxyl (-COOH), amino (-NH_2) boronate (B-O) and nitrogen

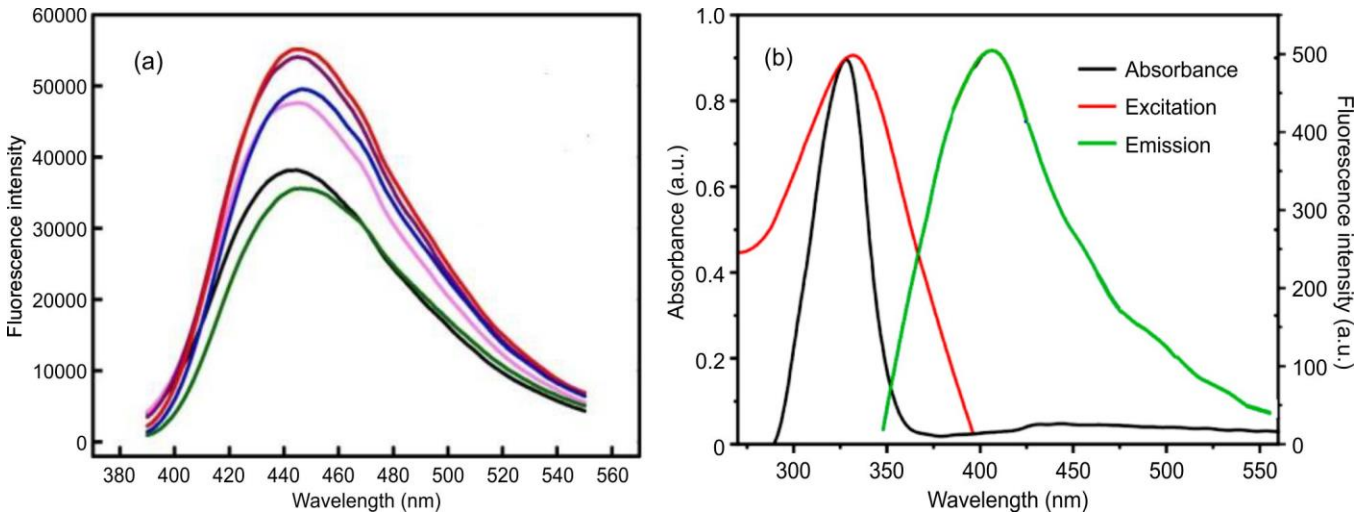

Fig. 3. (a) UV emission spectrum and (b) excitation dependent emission behaviour of N,B-CQDs

TABLE-1
COMPARATIVE DATA OF UNDOPED, SINGLE DOPED AND CO-DOPED CQDs

Sample	Quantum yield (%)	Lifetime (ns)	Emission (nm)	Relative intensity	Ref.
CQDs	9.2	2.1	410	Low	[28]
N-CQDs	15.8	3.0	415	Moderate	[29]
B-CQDs	12.6	2.8	418	Moderate	[30]
N,B-CQDs	32.0	7.42	420	High	–

doped carbon sites. The high positive charge and ability to accept electron nature of Fe^{3+} ions formed non fluorescence ground state complex with N,B-CQDs which is lead to static fluorescence quenching. The nitrogen dopants donate electron to Fe^{3+}, While boron dopants accept electron within the CQDs framework [33,34]. The dual acceptor-donor interaction accelerates photoinduced electron transfer, reduced radiative recombination and resulting in the intensity of fluorescence decreases.

Moreover, Fe^{3+} ions exhibit strong absorption in the ultra violet visible region which partially overlap with emission and excitation wavelengths of N,B-CQDs. This overlap introduced inner filter effect (IFE) and reduced fluorescence signal. A sensitive and concentration dependent fluorescence response is produced by the combined effect of static quenching, dynamic quenching and IFE [35].

pH responsive visual fluorescence sensing: N,B-CQDs showed excellent stability in alkaline solution. However, when the pH varied from 2 to 8, the fluorescence intensity gradually decreased and increased with increasing pH at 365 nm. Accordingly, the aqueous N,B-CQDs solution was pale yellow in presence of natural light, whereas under UV radiation, the emission colour changes from light blue to deep blue with increased intensity. The visual fluorescence changes provide a simple and easy platform for monitoring pH changes associated with corrosion initiation and propagation [36,37].

The establishment of a quantitative pH sensing method was enabled by the strong dependence of fluorescence intensity on pH. Under acidic conditions, the fluorescence intensity ratio (F/F_o) varied significantly and sigmoidal fitting analysis obtained a pK_a value of 4.75. Fluorescence intensity and pH showed excellent linear relationships with two linear response regions identified over the pH ranges of 2.0-4.8 and 5.2-7.6. These results confirmed the feasibility of using N,B-CQDs as a dual mode pH sensor based on both colorimetric and fluorescence responses, which is highly relevant for monitoring localised acidification during corrosion.

Reversibility is a critical requirement for continuous corrosion monitoring. In order to measure the fluorescence intensities by the pH of the N,B-CQDs solution was alternately adjusted between pH 2.0 and 7.0. The fluorescence signal demonstrated excellent reversibility within the pH range of 2.0-2.8 and complete recovery across several cycles. This property highlights the suitability of N,B-CQDs for real time and repetitive monitoring of pH changes in corrosion environments. Furthermore, a slight blue shift in the fluorescence emission peak was observed, when the pH ranges from 2.0 to 4.0. The emission peak is almost constant at the pH values between 5.0 and 8.0. Similarly, the UV-visible absorption spectra have an initial blue shift followed by a red shift and absorption intensity increases gradually. These two stage spectral changes are attributed to changes in the surface electronic states of N,B-CQDs, which are closely linked to the pK_a of the system. The pH response is mainly controlled by the protonation and deprotonation of surface carboxyl and amino groups (Fig. 4).

Fluorescence detection of Fe^{3+} as a corrosion monitor: The fluorescence response of N,B-CQDs on various metal ions was evaluated to assess their selectivity for corrosion related species. As shown in Fig. 5a, Fe^{3+} ions caused significance fluorescence quenching of N,B-CQDs whereas other metal ions produced only negligible intensity. Fig. 5b shows the fluorescence spectra of N,B-CQDs in the presence of different metal ions, confirming the high selectivity and sensitivity towards Fe^{3+} ions. The selectivity of N,B-CQDs toward Fe^{3+} can be attributed to the presence of boron containing functional groups on the CQDs surface [38]. Boron interact with hydroxyl groups to form sp^2 hybridised boronate species in aqueous environments. These rich boronate surfaces provide abundant coordination sites, which are commonly released during the corrosion processes. As a result, N,B-CQDs exhibit enhanced sensitivity and selectivity for Fe^{3+} compared to undoped CQDs. For quantitative detection, Fe^{3+} ions gradually added into the N,B-CQDs solutions. As shown in Fig.

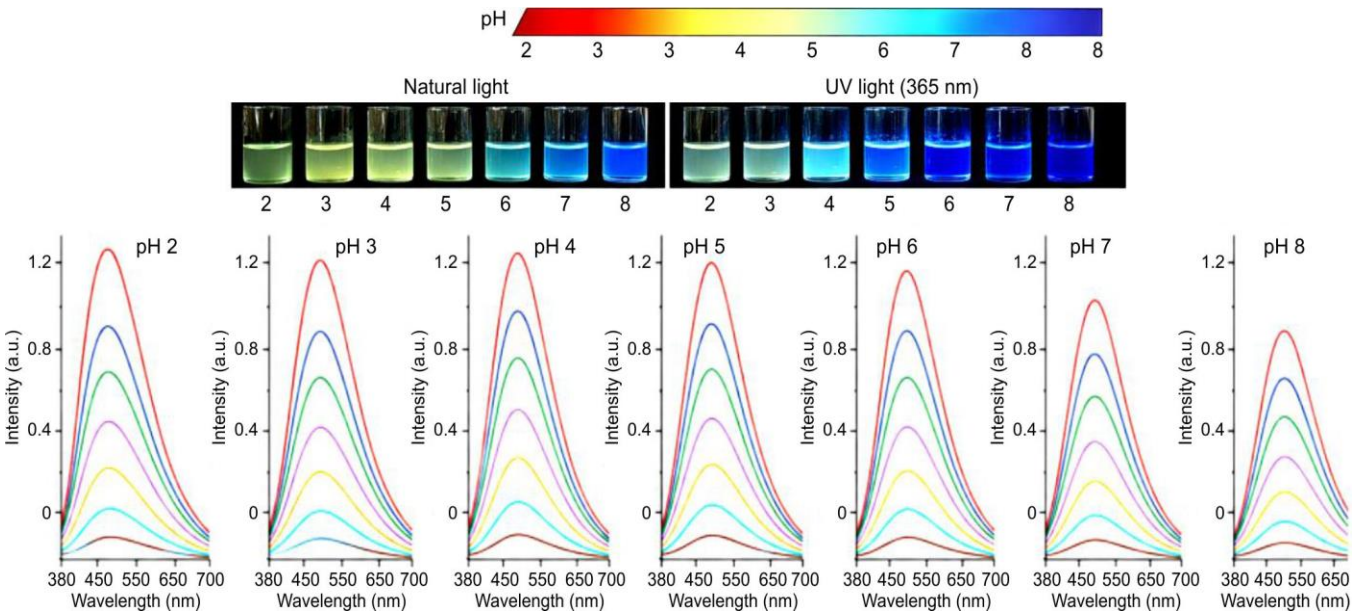

Fig. 4. pH dependent fluorescence behavior and emission spectral shift of the sample from pH 2 to 8 under natural and UV light

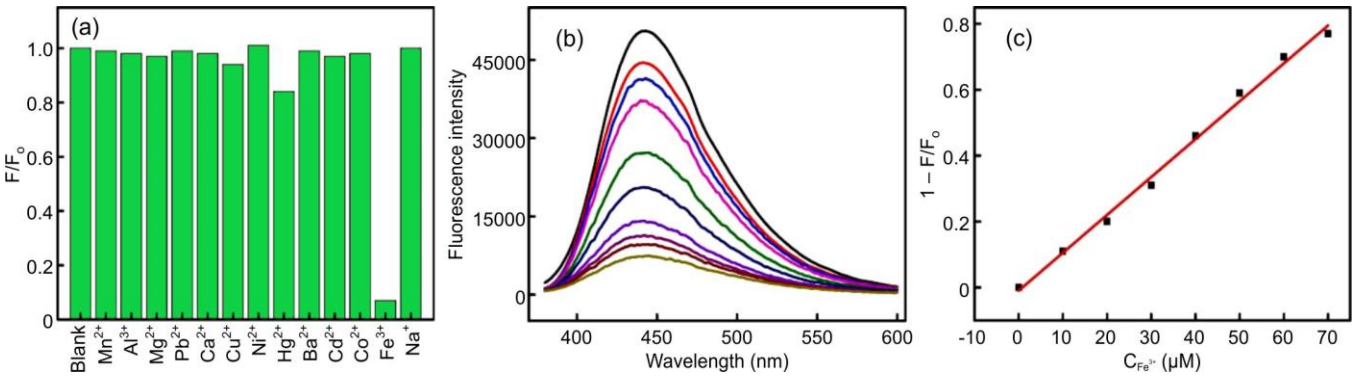

Fig. 5. (a) Ion selective study, (b) fluorescence spectrum of different concentrations of Fe^{3+} and (c) fluorescence intensity of N,B-CQDs

5b, the fluorescence intensity decreases which increases the Fe^{3+} ions concentration [39,40]. A linear relationship between the quenching coefficient ($1–F/F_o$) and Fe^{3+} concentration was obtained (Fig. 5c) with a corresponding regression coefficient correlation coefficient square (R^2) of 0.992. The limit of detection (LOD) was calculated by 3σ/S method is 0.044 μM. These results highlight that the N,B-CQDs are highly sensitive probes for detecting Fe^{3+} ions and making them suitable for early stage corrosion monitoring.

To analyse the practical applicability of the N,B-CQDs sensor for corrosion monitoring, Fe^{3+} ions released from the iron substrate which was served as a corrosion indicator. The fluorescence response of the N,B-CQDs probe was observed when controlled amounts of Fe^{3+} were added to simulate corrosion derived iron ion release. As summarised in Table-2, The sensor exhibited satisfactory recovery values ranging from 93.5% to 103.9%. The relative standard deviation (RSD) values were within 0.87-3.86%, which confirmed good repeatability and analytical precision. These low RSD values indicate that the fluorescence response of N,B-CQDs is stable and reliable for monitoring variations in iron ion concentration. The results indicate that the suggested fluorescence platform is capable of efficient monitoring in early stage corrosion through Fe^{3+} detection [41,42]. This method provides a sensitive, reproducible and nondestructive approach for real time corrosion assessments in iron based materials.

TABLE-2
RECOVERY AND PRECISION ANALYSIS OF Fe^{3+} IN TWO IRON TABLET USING N,B-CQDs

Sample	Added Fe^{3+} (μM)	Found Fe^{3+} (μM)	Recovery (%)	RSD (%)
Tablet 1	10	20.7 ± 0.8	93.5	3.86
Tablet 1	25	45.8 ± 0.4	101.8	0.87
Tablet 2	10	21.2 ± 0.7	99.5	3.30
Tablet 2	25	46.3 ± 0.5	103.9	1.05

Fluorescence quenching mechanism of N,B-CQDs to corrosion monitoring: The fluorescence quenching mechanism of N,B-CQDs was systematically investigated by electron transfer (ET), inner filter effect (IFE), fluorescence resonance energy transfer (FREF), dynamic quenching and static quen-ching. The absorption spectrum of N,B-CQDs was changed by the addition of Fe^{3+} ion, which indicate the new surface complex formation and excluding energy transfer mechanism, inner filter effect mechanism and fluorescence resonance energy transfer mechanism due to the lack Fe^{3+} ion absorption and N,B-CQDs emission (Fig. 6).

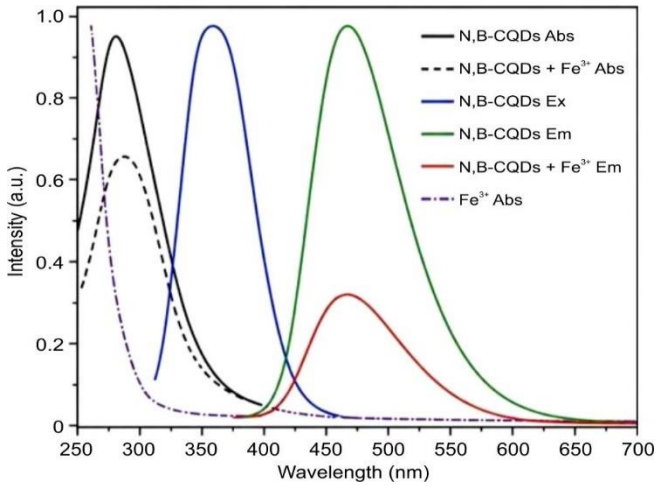

Fig. 6. Absorption spectra change of N,B-CQDs

Fluorescence lifetime measurements showed only slight changes from 7.22 ns to 7.42 ns after addition of Fe^{3+} ions, which indicate the quenching process was not governed by the single dynamic mechanism [43]. Zeta potential measurements revealed that the surface charge of N,B-CQDs shifted from -21.0 mV to +6.30 mV after Fe^{3+} binding which confirmed strong electrostatic interaction and complex formation (Fig. 7).

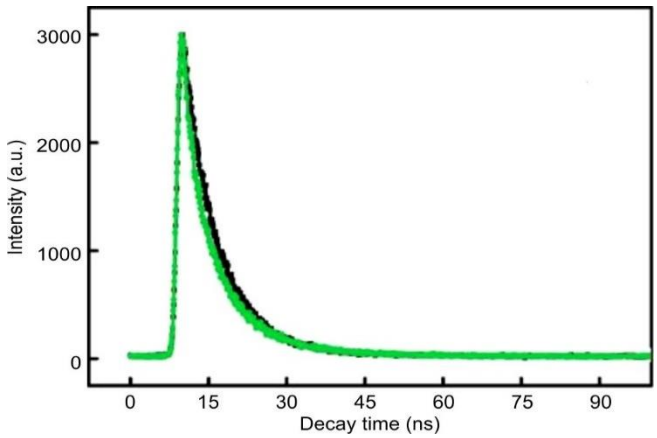

Fig. 7. UV-Visible absorption spectra of N,B-CQDs and N,B-CQDs-Fe^{3+}

The fluorescence quenching mechanism of N,B-CQDs toward Fe^{3+} ions was systematically investigated using Stern-Volmer analysis and temperature-dependent fluorescence studies (Fig. 8). The Stern-Volmer plot (Fig. 8a) exhibited a good linear relationship with a high correlation coefficient ($R^2 = 0.9928$), indicating a well-defined interaction between Fe^{3+} ions and the surface-active sites of the N,B-CQDs. In addition, the fluorescence quenching efficiency (F^o/F) gradually decreased with increasing temperature from 20 to 60 ºC, suggesting reduced stability of the Fe^{3+}–CQDs ground-state complex at elevated temperatures. Such behaviour is characteristic of a static quenching mechanism rather than dynamic collisional quenching. The observed quenching is therefore attributed predominantly to the formation of a non-fluorescent ground-state complex between Fe^{3+} ions and the O-, N- and B-containing functional groups present on the CQD surface. Furthermore, partial spectral overlap between the Fe^{3+} absorption band and the excitation spectrum of the N,B-CQDs indicates an additional contribution from the inner filter effect (IFE). These findings demonstrate that the fluorescence quenching process is mainly governed by static interaction with a minor contribution from IFE, thereby confirming the suitability of N,B-CQDs as sensitive fluorescence probes for Fe^{3+}-based corrosion monitoring [44].

Sensor performance evaluation

Repeatability: The repeatability of the N,B-CQDs was assessed by five independent measurements were conducted under identical experimental conditions. The fluorescence response toward Fe^{3+} ions, which act as corrosion indicators exhibited excellent consistency with a relative standard deviation (RSD) below 3.2%. This variation confirmed the high reproducibility and reliability of the sensing system that the developed N,B-CQDs sensor is well suited for corrosion related species in practical environments [45].

Long term stability: The long term stability of the N,B-CQDs sensor was evaluated over a period of 10 days under ambient storage conditions. The sensor retained more than 90% of its initial fluorescence intensity throughout the study, which indicated minimal signal degradation. The results confirmed that the N.B CQDs sensor possesses excellent durability and is suitable for continuous monitoring of corrosion processes in real environmental systems.

Selectivity: A comprehensive interference study was conducted to evaluate the selectivity of the N,B-CQDs sensor for Fe^{3+} ions in corrosion environments. Metal ions (Na^+, K^+, Ca^+, Mg^+, Zn^+), biomolecules (glucose, urea and citric acid), Industrial dyes (sunset yellow and rhodamine B) and common coexisting species were examined systematically. The fluorescence response exhibited minimal variation is less than 5% in the presence of these potential interferents. The result conforms the N,B-CQDs sensor retains high selectivity towards Fe^{3+} ions even in corrosion prone environments for corrosion monitoring.

Calibration and error analysis: Calibration curves were constructed using multiple independent measurements to ensure the accuracy and consistency of the analytical method for Fe^{3+} detection. The N,B-CQDs sensor exhibited excellent linearity over the studied concentration range, with correlation coefficients (R^2) exceeding 0.99. The low standard deviation across repeated measurements indicates high precision and reproducibility, while negligible instrumental error confirms the robustness of the sensing system [46]. These results validate the strong analytical performance of the developed sensor for quantitative corrosion monitoring in real samples.

Real sample analysis

Sample preparation: Real samples such as tap water, river water and industrial waste water were collected to evaluate practical applicability for corrosion prone environments. All the samples were filtered using a 0.22 μM membrane filter to remove suspended particles and impurities. Then, the filtered sample diluted with deionised water to minimize matrix

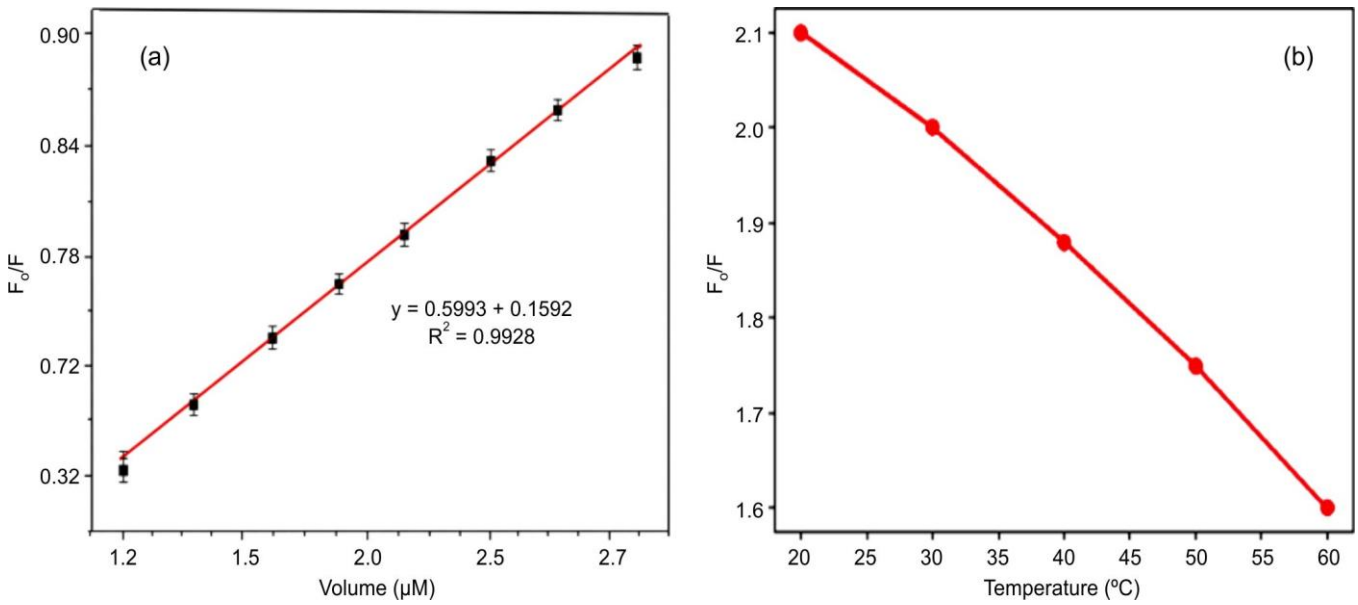

Fig. 8. (a) Stern-Volmer plot of N,B-CQDs-Fe^{3+} ions and (b) its effect of temperature on quenching efficiency

interference. This standardised sample preparation ensured fluorescence detection of Fe^{3+} ions during corrosion process in complex environmental systems.

Matrix effects evaluation: The matrix effects on sensor performance were assessed by standard addition method. Real samples were spiked with known concentrations of Fe^{3+} and the resulting fluorescence responses were measured. The recovery values ranges from 97.5% to 98.55% indicated high analytical accuracy and minimal matrix interference (Table-3). These results confirmed that the N,B-CQDs sensor is capable of reliably detect corrosion related Fe^{3+} ions in real samples [47].

TABLE-3
RECOVERY STUDY FOR CORROSION MONITORING

Added (μM)	Found (μM)	Recovery (%)
2	1.95	97.5
5	4.92	98.4
10	9.85	98.5

Comparison with standard techniques: The performance of the N,B-CQDs sensor was validated by comparison with atomic absorption spectroscopy (AAS), which is a standard technique for metal ion detection. The Fe^{3+} concentration determined using the N,B-CQDs sensor closely matched with the value of AAS (Table-4). This result confirmed the accuracy, reliability and practical applicability for corrosion monitoring in real samples.

TABLE-4
METHOD COMPARISON

Method	Fe^{3+} (μM)
Proposed N,B-CQDs sensor	4.92
Atomic absorption spectroscopy	5.00

Conclusion

Nitrogen and boron carbon quantum dots (N,B-CQDs) were successfully synthesised by hydrothermal method using citric acid, urea and borax. N,B-CQDs exhibited uniform morphology, strong fluorescence and high quantum yield. Their excellent photostability, salt tolerance, pH responses make them well suitable for corrosion monitoring application. A highly sensitive and selective fluorescence based Fe^{3+} detection was developed and achieved a linear detection range from 0.044-70 μM with a low detection limit of 0.044 μM. Static and Dynamic quenching processes were used to control the sensing mechanism. Furthermore, N,B-CQDs demonstrated effective pH sensing on corrosion environments. This study provides a strategy for designing heteroatom-doped CQDs as multifunctional fluorescence probes for corrosion monitoring.

CONFLICT OF INTEREST

The authors declare that there is no conflict of interests regarding the publication of this article.

DECLARATION OF AI-ASSISTED TECHNOLOGIES

During the preparation of this manuscript, the authors used an AI-assisted tool(s) to improve the language. The authors reviewed and edited the content and take full responsibility for the published work.

REFERENCES

1. S.N. Baker and G.A. Baker, *Angew. Chem. Int. Ed.*, **49**, 6726 (2010); https://doi.org/10.1002/anie.200906623
2. H. Li, Z. Kang, Y. Liu and S.T. Lee, *J. Mater. Chem.*, **22**, 24230 (2012); https://doi.org/10.1039/c2jm34690g
3. S.A. Umoren and M.M. Solomon, *J. Ind. Eng. Chem.*, **21**, 81 (2015); https://doi.org/10.1016/j.jiec.2014.09.033
4. A. Khan, A. Qurashi, W. Badeghaish, M.N. Noui-Mehidi and M.A. Aziz, *Sensors*, **20**, 6583 (2020); https://doi.org/10.3390/s20226583
5. Y.-P. Sun, B. Zhou, Y. Lin, W. Wang, K.A.S. Fernando, P. Pathak, M.J. Meziani, B.A. Harruff, X. Wang, H. Wang, P.G. Luo, H. Yang, M.E. Kose, B. Chen, L.M. Veca and S.-Y. Xie, *J. Am. Chem. Soc.*, **128**, 7756 (2006); https://doi.org/10.1021/ja062677d
6. Y. Dong, J. Shao, C. Chen, H. Li, R. Wang, Y. Chi, X. Lin and G. Chen, *Carbon*, **50**, 4738 (2012); https://doi.org/10.1016/j.carbon.2012.06.002
7. S. Zhu, Q. Meng, L. Wang, J. Zhang, Y. Song, H. Jin, K. Zhang, H. Sun, H. Wang and B. Yang, *Angew. Chem. Int. Ed.*, **52**, 3953 (2013); https://doi.org/10.1002/anie.201300519
8. S.Y. Lim, W. Shen and Z. Gao, *Chem. Soc. Rev.*, **44**, 362 (2015); https://doi.org/10.1039/C4CS00269E
9. K. Jiang, S. Sun, L. Zhang, Y. Lu, A. Wu, C. Cai and H. Lin, *Angew. Chem. Int. Ed.*, **54**, 5360 (2015); https://doi.org/10.1002/anie.201501193
10. Y. Wang and A. Hu, *J. Mater. Chem. C Mater. Opt. Electron. Devices*, **2**, 6921 (2014); https://doi.org/10.1039/C4TC00988F
11. J. Zhou, C. Booker, R. Li, X. Zhou, T.-K. Sham, X. Sun and Z. Ding, *J. Am. Chem. Soc.*, **129**, 744 (2007); https://doi.org/10.1021/ja0669070
12. H. Ding, S.-B. Yu, J.-S. Wei and H.-M. Xiong, *ACS Nano*, **10**, 484 (2016); https://doi.org/10.1021/acsnano.5b05406
13. S. Qu, X. Wang, Q. Lu, X. Liu and L. Wang, *Angew. Chem. Int. Ed.*, **51**, 12215 (2012); https://doi.org/10.1002/anie.201206791
14. R. Yadav and V. Lahariya, *J. Fluoresc.*, **35**, 12767 (2025); https://doi.org/10.1007/s10895-025-04487-5
15. H. Wu, L.-F. Pang, M.-J. Fu, X.-F. Guo, and H. Wang, *J. Pharm. Biomed. Anal.*, **180**, 113052 (2020); https://doi.org/10.1016/j.jpba.2019.113052
16. J. Liu, X. Liu, H. Luo and Y. Gao, *RSC Adv.*, **4**, 7648 (2014); https://doi.org/10.1039/C3RA47577H
17. X. Ren, F. Zhang, B. Guo, N. Gao and X. Zhang, *Nanomaterials*, **9**, 495 (2019); https://doi.org/10.3390/nano9040495
18. S.D. Dsouza, P.N. Jha, R. Basu, M.M. Shaijumon and S.K. Kailasa, *J. Photochem. Photobiol. A: Chem.*, **418**, 113393 (2021); https://doi.org/10.1016/j.jphotochem.2021.113393
19. M.E. Mohamed, B.A. Abd-El-Nabey and A. Ezzat, *Sci. Rep.*, **16**, 13897 (2026); https://doi.org/10.1038/s41598-026-47261-8
20. S. Zhao, M. Lan, X. Zhu, H. Xue, T.-W. Ng, X. Meng, C.-S. Lee, P. Wang and W. Zhang, *ACS Appl. Mater. Interfaces*, **7**, 17054 (2015); https://doi.org/10.1021/acsami.5b03228
21. K. Tolessa, M. Rademaker, B. De Baets and P. Boeckx, *Talanta*, **150**, 367 (2016); https://doi.org/10.1016/j.talanta.2015.12.039
22. M.A. Mousa, H.H. Abdelrahman, M.A. Fahmy, D.G. Ebrahim and A.H.E. Moustafa, *Sci. Rep.*, **13**, 12863 (2023); https://doi.org/10.1038/s41598-023-39490-y
23. S. Devi, A. Kaur, S. Sarkar, S. Vohra and S. Tyagi, *Integr. Ferroelectr.*, **186**, 32 (2018); https://doi.org/10.1080/10584587.2017.1369322
24. R. Kumar, V.B. Kumar and A. Gedanken, *Ultrason. Sonochem.*, **39**, 384 (2017); https://doi.org/10.1016/j.ultsonch.2017.05.002

25. H. Liu, K. Du, H. Sun, J. Wang, L. Zhang, Y. Chen, X. Li and M. Zhao, *Res. Chem. Intermed*., **49**, 4291 (2023); https://doi.org/10.1007/s11164-023-05106-3
26. J.R. Lakowicz, Principles of Fluorescence Spectroscopy, Springer, edn 3, pp. 277-330 (2006).
27. B. Valeur and M.N. Berberan-Santos, Molecular Fluorescence: Principles and Applications, Wiley-VCH, pp. 185-210 (2012).
28. P.K. Yadav, S. Chandra, V. Kumar, D. Kumar and S.H. Hasan, *Catalysts*, **13**, 422 (2023); https://doi.org/10.3390/catal13020422
29. J. Zheng, Y. Xie, Y. Wei, Y. Yang, X. Liu, Y. Chen and B. Xu, *Nanomaterials*, **10**, 82 (2020); https://doi.org/10.3390/nano10010082
30. Ç. Kırbıyık Kurukavak, T. Yılmaz, Ş. Çetin, M.M. Alqadasi, K.M. Al-Khawlany and M. Kuş, *Microelectron. Eng.*, **235**, 111465 (2021); https://doi.org/10.1016/j.mee.2020.111465
31. S. Hu, A. Trinchi, P. Atkin and I. Cole, *Angew. Chem. Int. Ed.*, **54**, 2970 (2015); https://doi.org/10.1002/anie.201411004
32. L. Cao, M.J. Meziani, S. Sahu and Y.-P. Sun, *Acc. Chem. Res*., **46**, 171 (2013); https://doi.org/10.1021/ar300128j
33. R. Juha and I. Alghoraibi, *Sci. Rep.*, **16**, 11816 (2026); https://doi.org/10.1038/s41598-026-41900-w
34. R.W. Revie and H.H. Uhlig, Corrosion and Corrosion Control, Wiley, edn, 4, pp. 85-110 (2008).
35. Y. Yang, T. Zou, Z. Wang, X. Xing, S. Peng, R. Zhao, X. Zhang and Y. Wang, *Nanomaterials*, **9**, 738 (2019); https://doi.org/10.3390/nano9050738
36. Q. Liu, C. Huang, G. Liu and B. Yu, *Sensors*, **18**, 2733 (2018); https://doi.org/10.3390/s18082733
37. Y. Liu, W. Li, P. Wu, C. Ma, X. Wu, M. Xu, S. Luo, Z. Xu and S. Liu, *Sens. Actuators B Chem.*, **281**, 34 (2019); https://doi.org/10.1016/j.snb.2018.10.075
38. S. Chen, Y. Hao, S. Liu, Y. Liu, Z. Zhang, M. Fang and L. Geng, *J. Saudi Chem. Soc.*, **28**, 101775 (2024); https://doi.org/10.1016/j.jscs.2023.101775
39. M.A. Issa, Z.Z. Abidin, S. Sobri, S.A. Rashid, M.A. Mahdi and N.A. Ibrahim, *Sci. Rep.* **10**, 11710 (2020); https://doi.org/10.1038/s41598-020-68390-8
40. R. Das, R. Bandyopadhyay and P. Pramanik, *Mater. Today Chem.*, **8**, 96 (2018); https://doi.org/10.1016/j.mtchem.2018.03.003
41. Y. Zhang, H. Qin, Y. Huang, F. Zhang, H. Liu, H. Liu, Z.J. Wang and R. Li, *J. Mater. Chem. B*, **9**, 4654 (2021); https://doi.org/10.1039/D1TB00371B
42. C.M. Singaravelu, X. Deschanels, C. Rey and J. Jérôme, *ChemPhotoChem*, **8**, e202400044 (2024); https://doi.org/10.1002/cptc.202400044
43. S. Zhu, Y. Song, X. Zhao, J. Shao, J. Zhang and B. Yang, *Nano Res.*, **8**, 355 (2015); https://doi.org/10.1007/s12274-014-0644-3
44. Z. Guo, X. Liu, H. Yu, F. Hou, S. Gao, L. Zhong, H. Xu, Y. Yu, J. Meng and R. Wang, *Spectrochim. Acta A Mol. Biomol. Spectrosc.*, **257**, 119774 (2021); https://doi.org/10.1016/j.saa.2021.119774
45. Y. Wang, Y. Liu, X. Liang, Z. Liu and Y. Yang, *Mikrochim. Acta*, **192**, 193 (2025); https://doi.org/10.1007/s00604-025-07051-x
46. Z. Yang, Y. Ma, Y. Liu, Q. Li, Z. Zhou and Z. Ren, *Chem. Eng. J.*, **315**, 403 (2017); https://doi.org/10.1016/j.cej.2017.01.042
47. T.T.K. Cuc, P.Q. Nhien, T.M. Khang, H.-Y. Chen, C.-H. Wu, B.T.B. Hue, Y.-K. Li, J.I. Wu and H.-C. Lin, *Dyes Pigments*, **197**, 109907 (2022); https://doi.org/10.1016/j.dyepig.2021.109907